Fast Demand Response with Variable Speed Thermal Loads - Towards Universal Modeling for Stability Assessment

Johanna Vorwerk*, Uros Markovic, Gabriela Hug
Power Systems Laboratory, ETH Zurich, Zurich, Switzerland
*vorwerk@eeh.ee.ethz.ch

***Abstract*—Besides batteries and renewable generation, thermal loads have been suggested in the literature as a potential solution to cope with the acceleration of power system dynamics caused by replacing conventional generators with inverter-interfaced units. While several models and control schemes exist, a general model suitable to represent different thermal load types with acceptable accuracy is missing. In this work, we derive a universal thermal load model capable of representing heat pumps, air conditioners, and refrigeration systems based on induction machines, brushless DC motors, or permanent magnet synchronous machines. To this end, we include detailed grid- and load-side inverter controls, a DC motor equivalent, and adequate load-side thermal dynamics. The performed time-domain studies for a low inertia system demonstrate the accuracy of the proposed universal model scenarios.**

***Index Terms*—Demand side resources, variable speed drives, low-inertia systems, differential-algebraic equations, dynamic load modeling**

I. Introduction

One challenge arising from the increasing share of renewable energy resources in modern power systems is the decline in system inertia and damping caused by replacing conventional synchronous machines with inverter-interfaced renewable resources. The literature proposes several solutions to cope with the resulting faster frequency dynamics. Besides batteries and inverter-based generation, recent research investigates control schemes for single or variable speed thermal loads to provide ancillary services in inverter-dominated systems [1].

The proposed continuous control schemes usually employ a droop control or virtual inertia emulation technique on a specific type of variable speed thermal load. For example, [2–4] develop models and control algorithms for variable speed heat pump systems, whereas [5] develops frequency support schemes for inverter air conditioning systems. Likewise, droop control with variable speed refrigeration is proposed in [6].

While most of the recent research focuses on the control design, the applied models differ in complexity. In [7–10], basic motor models that solely consider the motor efficiency are coupled with first- or second-order thermal dynamic models. Neglecting the inverter controls is appropriate for voltage stability studies but eliminates the fast controls dominant in frequency stability of inverter-dominated systems. Shorter time scales are included in [4, 11]. The authors develop advanced linear transfer function models for heat pumps that include motor and load-side inverter dynamics. Similarly, [2] proposes a detailed thermal network model and couples it to a transfer function motor and inverter model, and a detailed differential-algebraic equation model for stability studies with refrigeration systems is developed in [6]. Despite the numerous approaches, the representations either lack generality, are only suitable for one specific thermal load type, or apply simplifications that are insufficient for frequency stability studies.

The lack of a universal approach is addressed in [12–14], where high-order models for variable speed drive (VSD)-interfaced induction machines (IMs) that connect either constant or quadratic torque loads to the grid are developed. Despite the accurate representation of VSD and motor dynamics, the authors completely neglect the load side dynamics in order to adapt the model to any IM-based load. However, thermal loads are not always based on induction machines. For efficiency enhancement, the industry progressively employs brushless DC motors (BLDCs) and permanent magnet synchronous machines (PMSMs) for heating and cooling applications [15, 16].

This paper addresses the requirement for a universal load model needed for large-scale dynamic system studies of fast demand response in inverter-dominated power systems. As such, the contributions of the presented work are three-fold:

- We derive a universal thermal load model representing thermal loads of different types, i.e., heat pumps, air conditioners, and refrigeration systems, with sufficient detail for stability studies in low-inertia systems.
- Furthermore, the suggested model can express motor dynamics of IMs, BLDCs, and PMSMs. While mild assumptions that usually hold for heating and cooling applications are necessary to generalize the motor and inverter control sub-models, the grid-side rectifier controls, AC- and DC-side electric circuits are included with high detail.
- For each motor class, the universal model is compared and validated against a detailed representation in an infinite bus setup. The universal and detailed models are connected to a standard frequency droop control and a basic dynamic grid equivalent to illustrate and compare the impact on grid frequency.

The remainder of the paper is structured as follows: In Section II, we shortly discuss the limitations and recom-

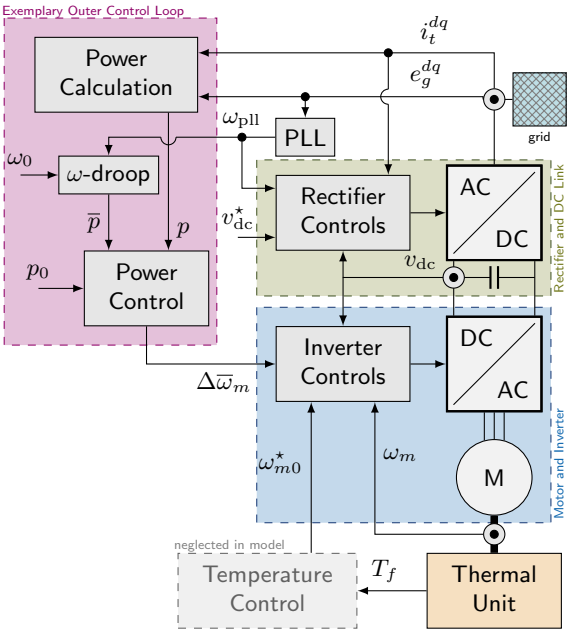

Fig. 1. Overview of the universal thermal load model.

mended use of the presented model. Then, Section III formulates the universal thermal load model, while Section IV demonstrates its accuracy through time-domain simulations. Additionally, the exemplary droop-control technique and applied grid equivalent are discussed. Finally, Section V concludes the paper.

II. Application, Recommended Use and Limitations

The suggested universal thermal load model is suitable to represent VSD-interfaced refrigeration, heat pumps, and air conditioning systems. However, several limitations apply due to the control algorithms and the mild assumptions required to arrive at a universal formulation.

The model is applicable to a unit with bi-directional, controllable front-end drives capable of controlling the DC-link voltage and the grid current, because it is necessary to control the power factor at the terminal. However, by adjusting the rectifier controls the model can be adapted for self-commutated front-end drives.

Even though the motivation was to apply the model in large-scale small-signal stability studies of inverter-dominated systems, it is not limited to this use case. For example, adding limits on the inverter and rectifier currents and the rotational speed or varying the power factor setpoint at the terminal provides a suitable formulation for transient and voltage stability studies.

In this work, we employ a basic frequency droop control scheme and synchronization technique to illustrate and validate the model's performance in case studies. Nonetheless, any synchronization, frequency, or voltage control scheme can be connected to the model as long as it acts on the external setpoints, i.e., the rotational speed or torque of the motor, the terminal power factor and the DC-link voltage.

III. Universal VSD Thermal Load Model

In Fig 1, a thermal unit is connected to the grid via a VSD and a motor. The grid-side rectifier maintains the DC link voltage v_{dc} and the power factor of the unit. On long time scales, the inverter controls manage the temperature in the controlled chamber by adjusting the motor's rotational speed. During power system transients, the synchronization unit, for example a phase-locked loop (PLL), detects a deviation from nominal frequency and passes it to the frequency droop controller. The latter computes a new terminal power reference $\overline{p}$ and forwards it to the power controller. Then, the steady-state rotational speed reference $\overline{\omega}_m$ is adjusted to achieve the required power change at the terminal.

The remainder of this section derives the universal VSD thermal load model in detail. The following conventions apply: First and second-order derivatives are denoted by $\dot{x}$ and $\ddot{x}$, respectively. The AC-side is formulated in a synchronously-rotating reference frame (SRF). Thus, AC-side quantities are denoted with $x^{dq} = x^d + jx^q$. While external system setpoints are marked by $x^\star$, internally computed references are indicated by $\overline{x}$.

A. Variable Speed Thermal Load

The thermal load comprises a controlled thermal chamber and a thermal cycle. Depending on the operation mode, i.e., cooling or heating, heat is either discharged from the chamber and transferred to the ambient or vice versa. Even though accurate models for thermal dynamics are available, they exceed the scope of the presented universal model. For dynamic grid studies, fast thermal dynamics are of primary interest. Thus, similar to the work in [4, 6], the applied thermal model includes the compressor and temperature dynamics within the chamber but neglects components that operate on longer time scales such as the temperature control, the evaporator and condenser. An overview of the VSD thermal load model is depicted in Fig. 2 and mathematically described in the following.

1) Thermal Chamber: In literature, equivalent thermal parameter (ETP) models for power systems ancillary service applications are either first- or second-order models [5–10, 17]. Even though the work in [9] demonstrates higher accuracy for a second-order model, a first-order differential equation is used in this work since the focus is on fast time scales and an equivalent model can be achieved by appropriately chosen parameters, as discussed in [9]. Thus, the temperature in the thermal chamber T_c is described by

$$\dot{T}_c = C^{-1} \left(U_m \left(T_o - T_c \right) - q_c \right), \tag{1}$$

where T_o denotes the ambient temperature, C and U_m express the thermal mass and the heat conductance, and q_c represents the heat transferred from or to the chamber by the thermal cycle. The latter is either positive or negative, depending on the operation mode.

2) Variable Speed Compressor: Inspired by the dynamic model of variable speed heat pumps in [2], the dynamics

of the compressor torque Γ_c and the heat transfer q_c are represented by the following mathematical representation:

$$\mathrm{COP} = c_2\omega_m^2 + c_1\omega_m + c_0, \tag{2a}$$
$$\Gamma_{c0} = \Gamma_{cn}\left(b_2\omega_m^2 + b_1\omega_m + b_0\right), \tag{2b}$$
$$q_{c0} = \mathrm{COP}\,\Gamma_{c0}\,\omega_m, \tag{2c}$$
$$\ddot{q}_c = n_0^q q_{c0} - d_1^q \dot{q}_c - d_0^q q_c, \tag{2d}$$
$$\Gamma_c = n_0^\Gamma \Gamma_{c0} - d_1^\Gamma \dot{\Gamma}_c - d_0^\Gamma q_c. \tag{2e}$$

Despite the linear torque relationship revealed for common variable speed compressors in [2], (2b) considers the steady-state torque Γ_0 as a second-order polynomial with parameters b_i and nominal torque Γ_{cn}. Correspondingly, the presented model is capable of representing different compressor types. Similarly, the coefficient of performance COP is a second-order polynomial with parameters c_i. The transient response for the heat transfer q_c and compressor torque Γ_c are second-order differential equations. All of the required parameters can be fitted with data sheets provided by thermal load manufacturers or by applying more detailed thermal models, such as [18].

B. Motor, Inverter and their Control

Since thermal loads operate with different motor types, a universal model requires the capability to represent all of them accurately. Preferably, the motor type can be switched without modifications. Thus, we employ a universal model that represents BLDCs, PMSMs, and IMs as DC machines. This section first presents the universal model considering a BLDC and then lists the required modifications to model PMSMs and IMs.

1) Universal Model: Fig. 3 depicts the universal motor model and its controls. The motor control receives a speed command $\overline{\omega}_m$ from the outer control loop and computes the reference for the torque producing current $\bar{i}_\Gamma$, that is equal to the armature current in case of a BLDC, with

$$\bar{i}_\Gamma = k_\omega\left[k_p^\omega\left(\overline{\omega}_m - \omega_m\right) + k_i^\omega \mu_\omega\right], \tag{3a}$$
$$\dot{\mu}_\omega = \overline{\omega}_m - \omega_m, \tag{3b}$$

where k_p^ω, k_i^ω are the PI control gains and ω_m represents the rotational speed. The speed control constant k_ω is required to adjust the control gains in case a torque control technique is employed, otherwise it is equal to one. The current reference is passed to a second PI controller that establishes the modulation signal for the pulse width modulator (PWM). Assuming ideal operation of the PWM and good tracking performance of the fast current control, the torque producing current i_Γ is of the form

$$\dot{i}_\Gamma = \omega_{cc}\left(\bar{i}_\Gamma - i_\Gamma\right), \tag{4}$$

where ω_{cc} is the current control's bandwidth. With the motor constant k_Γ the motor electric torque constitutes as $\Gamma_e = k_\Gamma i_\Gamma$ and the rotational speed is determined by the mismatch in torque, the motor inertia H and the friction coefficient b

$$\dot{\omega}_m = (2H)^{-1}\left(k_\Gamma i_\Gamma - \Gamma_c - b\omega_m\right). \tag{5}$$

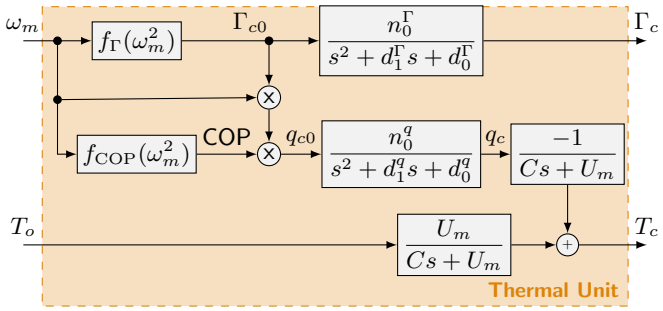

Fig. 2. Block diagram of the ETP chamber and the compressor model.

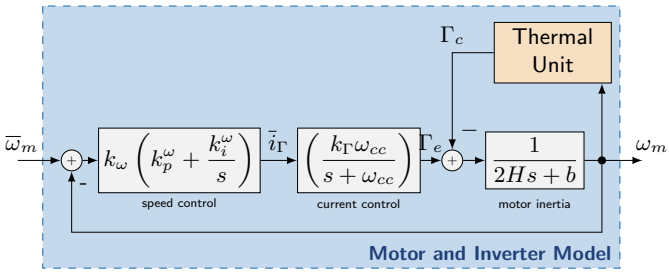

Fig. 3. Block diagram of the motor and inverter including their controls.

TABLE I
OVERVIEW OF ASSUMPTIONS AND MODIFICATIONS TO APPLY THE UNIVERSAL MODEL TO DIFFERENT MOTOR TYPES.

	BLDC	PMSM	IM
assumptions	good tracking of armature current control	good performance of decoupling current control, no flux weakening required	
i_Γ	armature current	q-axis stator current	
i_F	-	d-axis stator current	
$i_F^\star$	-	$i_d^\star = 0$	$i_d^\star = \psi_n \ell_m^{-1}$
k_Γ	1	ψ_n	ψ_n
k_ω	1	1	$k_\Gamma^{-1} = \psi_n^{-1}$

Finally, by neglecting inverter conversion losses and considering an averaged model the DC-link load current $i_{\mathrm{dc},2}$ is computed with

$$i_{\mathrm{dc},2} = \left(k_\Gamma \omega_m i_\Gamma + r_s i_s^2\right) v_{\mathrm{dc}}^{-1}, \tag{6}$$

where i_s is the stator current flowing through the stator resistance r_s. In case of a BLDC it holds that $i_s = i_\Gamma$.

2) Adjustments for IMs and PMSMs: The derived motor model is applicable for PMSMs and IMs if, for both motor types, field-oriented control is applied to decompose the stator current i_s into a torque-generating and a field-generating part, i.e. $i_s^2 = i_\Gamma^2 + i_F^2$. The torque producing ($i_\Gamma$) and field producing ($i_F$) currents are perpendicular, and an SRF is oriented such that $i^d = i_F$ and $i^q = i_\Gamma$. Since the field in a PMSM originates from permanent magnets, the field producing current is controlled to zero in this case, while for an IM, the nominal flux density ψ_n and magnetizing inductance ℓ_m determine the field current amplitude. Assuming proper operation of the decoupling current control strategy,

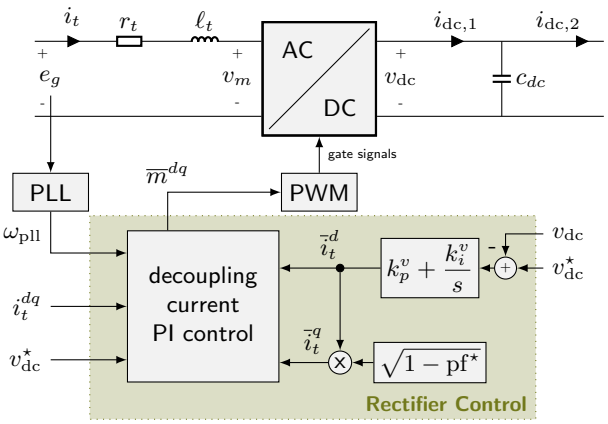

Fig. 4. Block diagram of the rectifier and its control scheme.

the d-axis is negligible ergo the presented universal model is pertinent [19, 20].

While PMSMs and BLDCs usually employ speed control, IMs are commonly operated through torque control. In this case, the PI-control on the speed mismatch outputs a torque reference $\overline{\Gamma}_e$ that is transformed into a current reference via $\bar{i}_\Gamma = \overline{\Gamma}_e \psi_n^{-1}$ [19,20]. Thus, for IMs $k_\omega = \psi_n^{-1}$ and $k_\Gamma = \psi_n$. Table I summarizes all assumptions and modifications.

C. Grid-side Rectifier Model and Control

The three-phase grid-side rectifier control maintains the DC-link voltage v_{dc}, the power factor pf, and the grid-side currents i_t^{dq} as detailed in [21]. For this purpose, a sequence of PI-controllers is employed as depicted in Fig. 4.

First, the voltage controller computes the d-axis terminal current reference $\bar{i}_t^d$

$$\bar{i}_t^d = k_p^v \left(v_{\mathrm{dc}}^\star - v_{\mathrm{dc}}\right) + k_i^v \mu_v, \tag{7a}$$

$$\dot{\mu}_v = v_{\mathrm{dc}}^\star - v_{\mathrm{dc}}, \tag{7b}$$

where k_p^v, k_i^v are the PI control gains, $v_{\mathrm{dc}}^\star$ is the DC-voltage setpoint and μ_v the integrator state. Using the reference power factor $\mathrm{pf}^\star$, the q-axis terminal current reference $\bar{i}_t^q$ follows

$$\bar{i}_t^q = \bar{i}_t^d \left(1 - \mathrm{pf}^\star\right)^{\frac{1}{2}}. \tag{8}$$

Finally, a decoupling current control strategy procures the reference modulation signals $\overline{m}^{dq}$ for PWM as outlined in [21] with

$$-\overline{m}^{dq} = k_p^c \left(\bar{i}_t^{dq} - i_t^{dq}\right) + k_i^c \mu_c^{dq} + j\omega_{\mathrm{pll}} \ell_t i_t^{dq} {v_{\mathrm{dc}}^\star}^{-1}, \tag{9a}$$

$$\dot{\mu}_c^{dq} = \bar{i}_t^{dq} - i_t^{dq}, \tag{9b}$$

where k_p^c, k_i^c are the PI-control gains, ω_{pll} is the estimated frequency, ℓ_t the terminal inductance, and μ_c^{dq} are the integrator states. Since PWM is assumed to have ideal operation, the modulation signal is equal to its reference $m^{dq} = \overline{m}^{dq}$.

D. Electrical System Dynamics

The VSD is connected to the grid via an impedance (r_t, ℓ_t). Thus, when neglecting switching losses and considering an averaged model of the rectifier, the terminal current dynamics are of the form

$$\dot{i}_t^{dq} = \omega_b \ell_t^{-1} \left(v_t^{dq} - m^{dq} v_{\mathrm{dc}} - r_t i_t^{dq}\right) - j\omega_b \omega_g i_t^{dq}, \tag{10}$$

as shown in [21], where ω_b is the base frequency. Moreover, the common DC-side dynamics across the DC-link capacitor c_{dc} can be derived as

$$\dot{v}_{\mathrm{dc}} = \omega_b c_{\mathrm{dc}}^{-1} \left(m^d i_t^d + m^q i_t^q - i_{\mathrm{dc},2}\right). \tag{11}$$

The terminal power p of the unit is:

$$p = e_g^d i_t^d + e_g^q i_t^q, \tag{12}$$

where e_g^{dq} is the grid voltage and i_t^{dq} the terminal current.

IV. Validation with Case Studies

Case studies are performed to assess the accuracy of the universal thermal load model for all motor types. To this end, six sets of time-domain simulations are performed to compare the universal model outcome to a detailed version for each motor type. Before presenting the results of the case studies, this section first discusses the simulation setup, including the applied exemplary outer control loop and external power system, and the high-order models used for comparison.

A. Case Study Setup

An overview of the system setup for the case study is given in Fig. 5. A standard PLL and frequency droop control technique are added to illustrate the contribution of a fast demand response scheme on the mains frequency. Moreover, a thermal load aggregation with n_s units is connected to an infinite bus. The case study parameters are listed in Table II. Note that, although the universal model could represent the heating and cooling of chambers with different sizes and thermal properties, the presented case studies all share the same thermal parameters for simplification and comparison purposes.

1) Exemplary Outer Control Loop: A classic PLL estimates the grid frequency ω_g. Then, the estimate ω_{pll} is compared to the nominal frequency ω_0 and a frequency droop d_f is applied to establish the required terminal power reference $\overline{p}$. The latter is passed to the power PI-controller that outputs the required change in rotational speed of the motor. The entire system is described by the algebraic and differential equations as given by

$$\Delta\dot{\theta}_{\mathrm{pll}} = (\omega_0 - \omega_{\mathrm{pll}})\omega_b, \tag{13a}$$

$$\dot{\mu}_{\mathrm{pll}} = v_g^q, \tag{13b}$$

$$\dot{\mu}_p = \overline{p} - p, \tag{13c}$$

$$\omega_{\mathrm{pll}} = \omega_0 + k_p^{\mathrm{pll}} v_g^q + k_i^{\mathrm{pll}} \mu_{\mathrm{pll}}, \tag{13d}$$

$$v_g^q = -e_g^d \sin(\Delta\theta) + e_g^q \cos(\Delta\theta), \tag{13e}$$

$$\overline{p} = p_0 + d_f \left(\omega_{\mathrm{pll}} - \omega_0\right), \tag{13f}$$

$$\overline{\omega}_m = \omega_{m0}^\star + k_p^p \left(\overline{p} - p\right) + k_i^p \mu_p. \tag{13g}$$

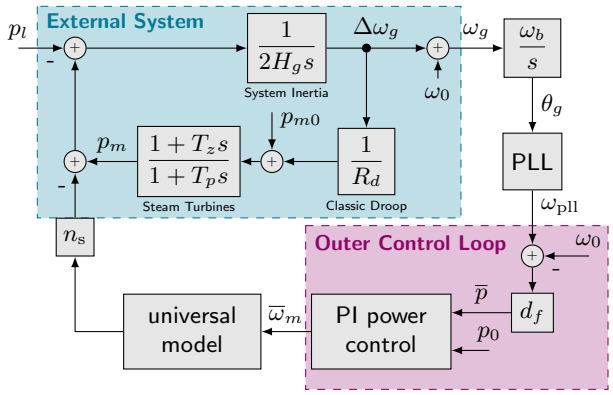

Fig. 5. Setup for validation test including the external power system and the exemplary outer control loop.

For a detailed description of the modeling process and parameter declaration we refer the reader to [6].

2) External Power System: To demonstrate the usability for frequency control and the effect on the grid, the units are connected to an infinite bus that represents frequency dynamics by the swing equation and primary frequency control through an appropriate equivalent as suggested in [22], applied in [6, 11] and included in Fig. 5. A mathematical representation is given by

$$\dot{p}_m = -\frac{1}{T_p}(p_m - p_{m0}) - \frac{1}{R_d T_p}\overbrace{(\omega_g - \omega_0)}^{\Delta\omega_g} - \frac{T_z}{2H_g R_d T_p}(p_m - p_l - n_s p), \tag{14a}$$

$$\Delta\dot{\omega}_g = \frac{1}{2H_g}(p_m - n_s p - p_l), \tag{14b}$$

$$\dot{\theta}_g = \omega_g \omega_b, \tag{14c}$$

and the chosen parameterization can be found in [6]. The individual thermal units are scaled to account for 5% of the power systems pre-disturbance load as indicated in Table II.

3) High-Order Models: The universal load model is compared to high-order version for each motor option. The following additional elements were included in the detailed formulations: Instead of assuming ideal current tracking of the BLDC, the motor current control is accurately modeled. Then, with the power balance across the inverter, the DC-link load current is computed as $i_{\mathrm{dc},2} = v_{\mathrm{dc}}^{-1}\left(v_m^d i_s^d + v_m^q i_s^q\right)$, where v_m^{dq} is the stator voltage.

Similarly, in case of the PMSM and IM, the load-side decoupling current control, the stator currents and flux linkages are modeled as described in [19, 20]. The DC-side load current is computed in the same fashion as for the BLDC. For the tuning of the inverter controls the symmetric optimum criterion was applied. Note, that the same control bandwidths were applied to the reduced-order models.

B. Time-Domain Simulation Results

One set of time-domain simulations is performed for each motor type, both with universal and detailed representation. Each of the systems is subjected to a 0.1 p.u. reduction in power system background load. Fig. 6 demonstrates the performance of the BLDC, PMSM and IM based detailed and universal models for selected states and algebraic variables. Most importantly, the presented simulation results show the overlap of the full and general models for each motor type. Only for the terminal power of the IM based thermal unit a slight mismatch occurs. It originates from the computation of the motor loss with $r_s i_s^2$ which is not exact for an IM, but cannot be improved without significantly complicating the universal model. Moreover, the mismatch is small and the presented universal model is more accurate than the IM models presented in [4, 10].

Furthermore, Fig. 6 suggests similar behavior of the grid frequency for all three motor types even though the current and speed transients differ. Thereby, the results confirm the findings in [11] by implying that the grid-side dynamics and mainly the PLL influence the grid frequency response rather than the load-side dynamics. Nonetheless, further investigations are required to validate this claim.

V. Conclusions

In this paper, a universal thermal load model suitable for variable-speed heating and cooling systems based on IMs, BLDCs, and PMSMs was derived. Mild assumptions that allow the IM and PMSM to be modeled as a DC machine apply. Otherwise, all system components are incorporated with the order of detail suitable for dynamic studies in inverter-dominated systems.

A case study demonstrates the accurate performance of the universal thermal load model by comparing it to detailed representations for each motor type. Thereby, it validates the assumptions required to apply the reduced-order motor models. Solely in the case of IM-based thermal loads, a slight but acceptable mismatch of the power at the terminal during transients occurs.

The three thermal loads, i.e., BLDC-based, PMSM-based, and IM-based refrigeration, show similar grid frequency responses in the case studies. In particular, the frequency nadir is equal, although the rotational speed and torque current transients differ. Therefore, the conducted case study

TABLE II
System parameters. Thermal and grid-side rectifier parameters where taken from [6]. Motor parameters were taken from examples in [19, 20]. All parameters were transformed into per unit.

Grid Equivalent		**PII**	
H	$0.5\,\mathrm{s}$	$k_{p,pll}$	$0.4\,\mathrm{p.u.}$
R_d	$0.02\,\mathrm{p.u.}$	$k_{i,pll}$	$4.69\,\mathrm{p.u.\,s^{-1}}$
D_l	$0.2\,\mathrm{p.u.}$	**Frequency Droop**	
T_z	$0.5\,\mathrm{s}$	d_f	$50\,\mathrm{p.u.}$
T_p	$9\,\mathrm{s}$	**Nominal Power**	
base power	$200\,\mathrm{MW}$	IM	$2.5\,\mathrm{kW}$
base frequency	$50\,\mathrm{Hz}$	PMSM	$1.3\,\mathrm{kW}$
background load	$0.95\,\mathrm{p.u.}$	BLDC	$3.3\,\mathrm{kW}$

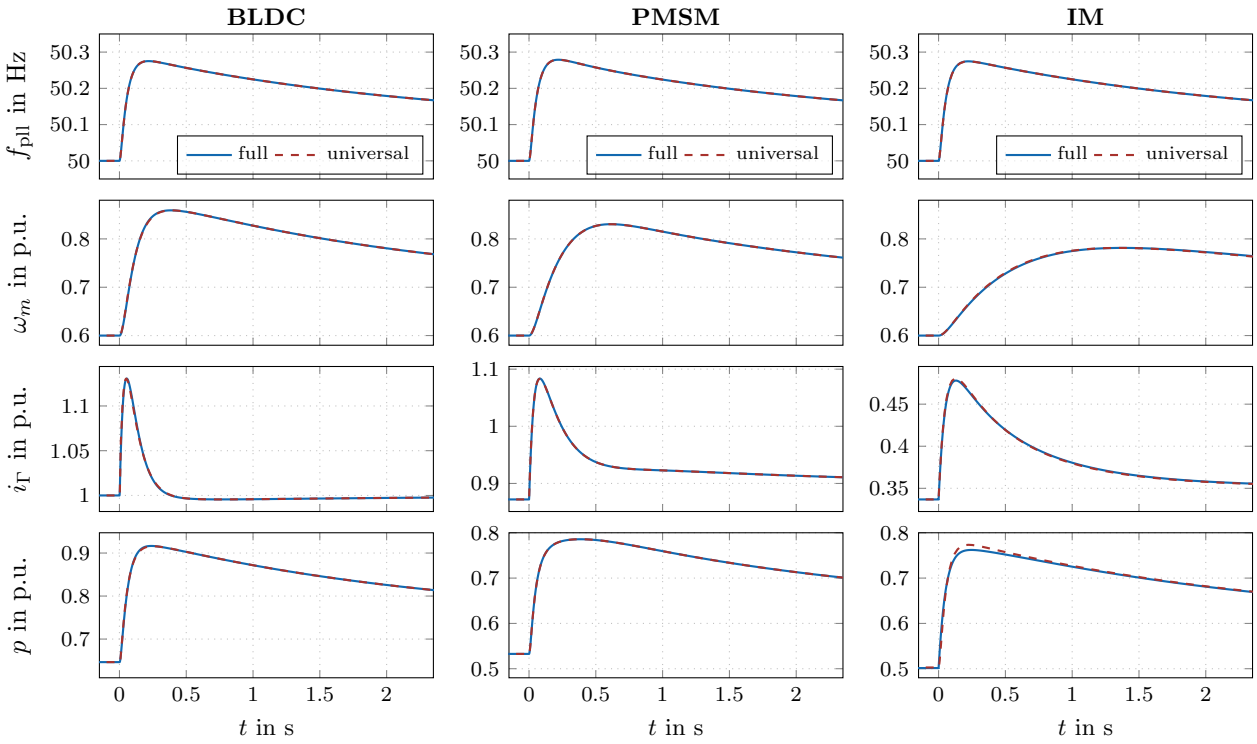

Fig. 6. Time domain validation of the universal model against each of the full-order models for BLDC-based units on the left, PMSM-based units in the middle and IM-based units on the right for a 0.1 p.u. decrease in power system background load. While the abscissa for all plots as well as the ordinate for the frequency and rotational speed share the same scaling, note the different scaling of the ordinate in the power and current plots.

indicates that outer loop controls dictate the grid-side response of the system. However, this might change when the units' converter and motor limits, which remain to be included in the model, are added.

References

[1] H. Karbouj, Z. H. Rather, D. Flynn, and H. W. Qazi, "Non-synchronous fast frequency reserves in renewable energy integrated power systems: A critical review," *Int. J. Electr. Power Energy Syst.*, vol. 106, pp. 488 – 501, 2019.

[2] Y.-J. Kim, L. K. Norford, and J. L. Kirtley, "Modeling and Analysis of a Variable Speed Heat Pump for Frequency Regulation Through Direct Load Control," *IEEE Trans. Power Syst.*, vol. 30, no. 1, pp. 397–408, Jan. 2015.

[3] Y.-J. Kim, E. Fuentes, and L. K. Norford, "Experimental Study of Grid Frequency Regulation Ancillary Service of a Variable Speed Heat Pump," *IEEE Trans. Power Syst.*, vol. 31, no. 4, pp. 3090–3099, 2016.

[4] I. Ibrahim, C. O'Loughlin, and T. O'Donnell, "Virtual Inertia Control of Variable Speed Heat Pumps for the Provision of Frequency Support," *Energies*, vol. 13, no. 8, p. 1863, 2020.

[5] H. Hui, Y. Ding, and M. Zheng, "Equivalent Modeling of Inverter Air Conditioners for Providing Frequency Regulation Service," *IEEE Trans. Ind. Electron.*, vol. 66, no. 2, pp. 1413–1423, Feb. 2019.

[6] J. Vorwerk, U. Markovic, P. Aristidou, E. Vrettos, and G. Hug, "Modelling of variable-speed refrigeration for fast-frequency control in low-inertia systems," *IET Smart Grid*, vol. 3, no. 6, pp. 924–936, 2020.

[7] N. Mahdavi and J. H. Braslavsky, "Modelling and control of ensembles of variable-speed air conditioning loads for demand response," *IEEE Trans. Smart Grid*, May 2020.

[8] Y. Che, J. Yang, Y. Zhou, Y. Zhao, W. He, and J. Wu, "Demand response from the control of aggregated inverter air conditioners," *IEEE Access*, vol. 7, pp. 88 163–88 173, 2019.

[9] W. Zhang, J. Lian, C.-Y. Chang, and K. Kalsi, "Aggregated Modeling and Control of Air Conditioning Loads for Demand Response," *IEEE Trans. Power Syst.*, vol. 28, no. 4, pp. 4655–4664, 2013.

[10] J. García, J. Víquez, J. Incer, F. Escobar, P. Aristidou, and G. Valverde, "Modeling Framework and Coordination of DER and Flexible Loads for Ancillary Service Provision," in *Proceedings of the 54th Hawaii International Conference on System Sciences*. Hawaii: HICSS, 2021.

[11] J. Vorwerk, U. Markovic, and G. Hug, "Comparing the damping capabilities of different fast-frequency controlled demand technologies," in *IEEE PES PowerTech 2021*, Madrid.

[12] D. Chakravorty, B. Chaudhuri, and S. Y. R. Hui, "Rapid frequency response from smart loads in great britain power system," *IEEE Trans. Smart Grid*, vol. 8, no. 5, pp. 2160–2169, 2017.

[13] R. Azizipanah-Abarghooee and M. Malekpour, "Smart induction motor variable frequency drives for primary frequency regulation," *IEEE Trans. Energy Convers.*, vol. 35, no. 1, pp. 1–10, 2020.

[14] M. Malekpour, R. Azizipanah-Abarghooee, F. Teng, G. Strbac, and V. Terzija, "Fast Frequency Response From Smart Induction Motor Variable Speed Drives," *IEEE Trans. Power Syst.*, vol. 35, no. 2, pp. 997–1008, 2020.

[15] "Brushless DC Motor Market Size, Share & Trends Analysis Report," Grand View Research, Tech. Rep., 2021.

[16] N. Kostora, "The Evolution of Permanent Magnet Synchronous Motors," *The NEWS*, 02 2017.

[17] E. Vrettos, C. Ziras, and G. Andersson, "Fast and reliable primary frequency reserves from refrigerators with decentralized stochastic control," *IEEE Trans. Power Sys.*, vol. 32, no. 4, pp. 2924–2941, Jul. 2017.

[18] R. Koury, L. Machado, and K. Ismail, "Numerical simulation of a variable speed refrigeration system," *IJR*, vol. 24, no. 2, pp. 192–200, Mar. 2001.

[19] R. Krishnan, *Electric Motor Drives: Modeling, Analysis and Control*. Pearson, 2001.

[20] S.-H. Kim, *Electric Motor Control: DC, AC, and BLDC Motors*. Elsevier, 2017.

[21] F. Blaabjerg, *Control of Power Electronic Converters and Systems*. Elsevier, 2018.

[22] T. Weckesser and T. Van Cutsem, "Equivalent to represent inertial and primary frequency control effects of an external system," *IET Gener. Transm. Distrib.*, vol. 11, no. 14, pp. 3467–3474, 2017.